

2.3. POWDER AND RELATED TECHNIQUES: X-RAY TECHNIQUES

diffraction (Reynolds, 1989), instrumentation, specimen preparation, profile fitting, synchrotron and neutron methods. A recent book by Jenkins & Snyder (1996) gives a useful comprehensive account of basic methods and practices in powder diffractometry.

Papers presented at international symposia on powder diffraction describe advances in the field (Block & Hubbard, 1980; *Australian Journal of Physics*, 1988; Bojarski & Bořd, 1979; Bish & Post, 1989; Prince & Stalick, 1992). Papers on the theory and new methods and applications are published in the *Journal of Applied Crystallography*. *Powder Diffraction* started in 1986 and contains powder data and papers on instrumentation and methods. Papers presented at the Annual Denver Conference on Applications of X-ray Analysis have been published yearly since 1957 as separate volumes entitled *Advances in X-Ray Analysis*, by Plenum Press. Volume 37 of the series was published in 1994. These volumes contain papers that are roughly equally divided between X-ray powder diffraction and fluorescence analysis. This extensive source describes many types of instrumentation, methods and applications. The *Norelco Reporter* has been published several times a year since 1954 and contains original articles and reprints of papers on powder diffraction, fluorescence analysis, and electron microscopy. There are other 'house journals' published by Rigaku, Siemens, and other X-ray companies. A history of the powder method in the USA was written by Parrish (1983).

The following description includes only the most frequently used methods. The divergent beam from X-ray tubes is best used with focusing geometries, and synchrotron radiation with parallel-beam optics.

2.3.1. Focusing diffractometer geometries

The critical elements in the basic geometries of the principal focusing diffractometers used with X-ray tubes are illustrated schematically in Fig. 2.3.1.1. The six arrangements are described below in paragraphs (a) to (f) corresponding to the subdivisions of Fig. 2.3.1.1. The most frequently used methods are illustrated in (a) and (b). The abbreviations used are $S(R)$ for

the specimen set for reflection, $S(T)$ for a transmission specimen, and M refers to a focusing reflection monochromator. The letters are arranged in order of the beam direction. The detector rotates around the diffractometer axis at twice the speed of the specimen in the θ - 2θ scanning used in (a) to (e). In the Seemann-Bohlin geometry (S - B), the specimen is stationary and the detector rotates around the focusing circle in scanning the pattern (f). The line focus of the X-ray tube is used in all cases.

The monochromator is either symmetrical, with the lattice planes parallel to the crystal surface, or asymmetric with the lattice planes inclined at a small angle to the surface to shorten one of the focal-length distances. Placing the monochromator in the diffracted beam has the important advantage of eliminating specimen fluorescence. It also simplifies shielding the detector if the specimen is radioactive. The monochromator in the incident beam reduces fluorescence and radiation damage to the specimen by removing the continuous X-ray spectrum. When the diffracted beam is defined by the receiving slit as in (b) and (c), highly oriented pyrolytic graphite (placed in front of the detector) is generally used to obtain high intensity. In the (d) and (e) geometries, a high-quality bent crystal such as silicon or quartz is necessary to achieve good focusing.

(a) $S(R)$: The aperture of the incident divergent beam from the line focus of the X-ray tube F is limited by the entrance slit ES and the reflection from the specimen converges ('focuses') on the receiving slit RS . The intensity is determined by the ES and RS and the profile width is determined mainly by the RS width. The parallel slits PS in the incident and diffracted beams limit the axial divergence.

(b) $S(R)/M$: Same as (a) with the addition of the symmetrical monochromator (usually graphite) to record only the characteristic radiation. ES and RS have the same rôle as in (a), and only the incident PS are required.

(c) $M/S(R)$: Using an incident-beam monochromator, the slit at F' determines the effective source size and divergence of the beam striking the specimen, and RS limits the profile width.

(d) $S(T)/M$: The divergent incident beam continues to diverge after diffraction from the transmission specimen and the asymmetric monochromator focuses the beam on the detector.

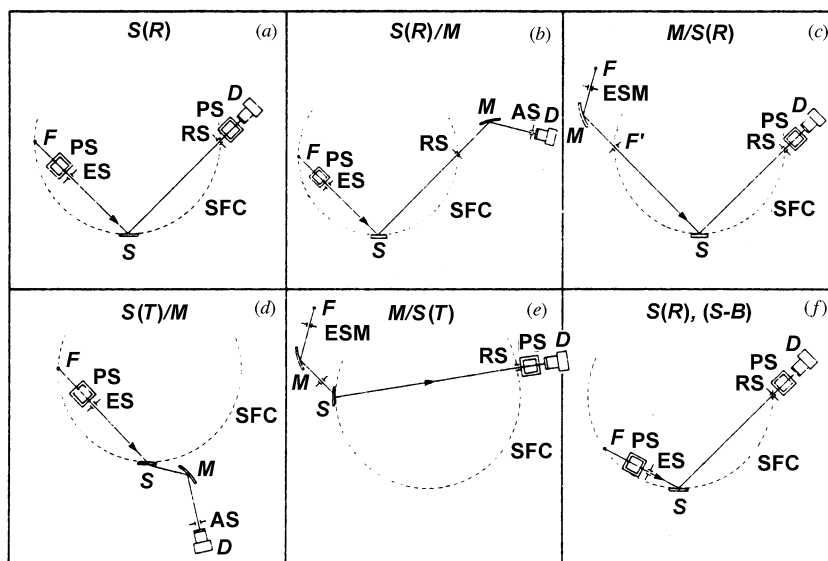


Fig. 2.3.1.1. Basic arrangements of focusing diffractometer methods. Simplified and not to scale; detailed drawings shown in later figures. (a)–(e) operate with θ - 2θ scanning; (f) fixed specimen with detector scanning. F line focus of X-ray tube (normal to plane of drawings), F' focus of incident-beam monochromator, PS parallel slits (to limit axial divergence), ES entrance (divergence) slit, ESM entrance slit for monochromator, S specimen, RS receiving slit, AS antiscatter slit, D detector, SFC specimen focusing circle, M focusing monochromator. Other symbols described in text.

2. DIFFRACTION GEOMETRY AND ITS PRACTICAL REALIZATION

M and D rotate around S in θ - 2θ scanning and the profile width is determined by the monochromator. Only the forward-reflection region can be recorded.

(e) $M/S(T)$: This is the diffractometer equivalent of the Guinier camera. A symmetric or asymmetric monochromator is used in the incident beam and the profile width is determined by the RS . The incident-beam divergence is limited by ESM.

(f) $S(R),(S-B)$: The reflections are focused on a fixed-radius circle which moves the detector around the focusing circle and always points it to the fixed specimen. The angular range is limited (normally 30 - $240^\circ 2\theta$) and can be changed by moving the specimen and diffractometer to different positions. The profile width is determined by ES and RS. The same geometry is used with an incident- or diffracted-beam focusing monochromator.

The interaction of the X-ray beam with the specimen varies in different geometries and this may have important consequences on the results, as will be described later. When a reflection specimen is used in θ - 2θ or θ - θ scanning, only those crystallites whose lattice planes are oriented nearly parallel to the specimen surface can reflect (Fig. 2.3.1.2) (Parrish, 1974). A transmission specimen in θ - 2θ scanning permits reflections only from planes nearly normal to the surface. In the S - B case, reflections can occur from planes inclined over a range of about 45° to the surface. Transmission specimens must, of course, be mounted on

X-ray-transparent substrates. Jenkins (1989) has reviewed the instrumentation and experimental procedures.

2.3.1.1. Conventional reflection specimen, θ - 2θ scan

The reflection specimen with θ - 2θ scanning in the focusing arrangement shown in Fig. 2.3.1.3 is the most widely used powder diffraction method. It is estimated that about 10 000 to 15 000 of these diffractometers have been sold since they were introduced in 1948, which makes it the most widely used X-ray crystallographic instrument. Some authors have called it the Bragg-Brentano para-focusing method (Bragg, 1921; Brentano, 1946), but the X-ray optics (described below) are significantly different from the methods and instruments described by these authors.

The X-ray tube spot focus was first used as the source and gave broad reflections. A narrow entrance slit improved the resolution but caused a large loss of intensity. Early diffractometers were described by LeGalley (1935), Lindemann & Trost (1940), and Bleekma, Kloos & DiGiovanni (1948); see Parrish (1983). The use of the line focus with parallel slits to limit axial divergence was developed in the late 1940's and gave much higher resolution. A collection of papers by Parrish and co-workers (Parrish, 1965) and Klug & Alexander (1974) describe details of the instrumentation and method.

2.3.1.1.1. Geometrical instrument parameters

The powder diffractometer is basically a single-axis goniometer with a large-diameter precision gear and worm drive. The detector and receiving-slit assembly are mounted on an arm attached to the gear in a radial position. The specimen is mounted in a holder carried by a shaft precisely positioned at the centre of the gear. $2/1$ reduction gears drive the specimen post at one-half the speed of the detector. Some diffractometers have two large gears, making it possible to drive only the detector with the specimen fixed or *vice versa*, or to use $2/1$ scanning. Synchronous motors have been used for continuous scanning for ratemeter recording and stepping motors for step-scanning with computer control.

The geometry of the method requires that the axis of rotation of the diffractometer be parallel to the X-ray tube focal line to obtain maximum intensity and resolution. The target is normal to the long axis of the tube; vertically mounted tubes require a diffractometer that scans in the vertical plane while a horizontal tube requires a horizontal diffractometer. The X-ray optics are the same for both. The incident angle θ and the reflection angle 2θ are defined with respect to the central ray that passes through the diffractometer axis of rotation O .

The axis of rotation of the specimen is the central axis of the main gear of the diffractometer, as shown in Fig. 2.3.1.3. The centre of the specimen is equidistant from the source F and receiving slit RS . The instrument radius $R_{DC} = F - O = O - RS$. The radius of commercial instruments is in the range 150 to 250 mm, with 185 mm most common. Changing the radius affects the instrument parameters and a number of the aberrations. Larger radii have been used to obtain higher resolution and better profile shapes. For example, the asymmetric broadening caused by axial divergence is decreased because the chord of the diffraction cone intercepted by the receiving slit has less curvature. However, if the same entrance slit is used, moving the specimen further from the source proportionately increases the length of specimen irradiated and decreases the intensity.

The imaginary specimen focusing circle SFC passes through F , O and the middle of RS and its radius varies with θ :

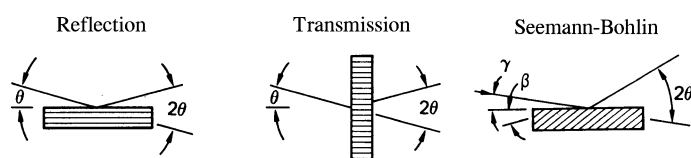


Fig. 2.3.1.2. Specimen orientation for three diffractometer geometries. With θ - 2θ scanning, diffraction is possible only from planes nearly parallel to the reflection specimen surface (left), and from planes nearly normal to the transmission specimen surface (middle), and from planes inclined different amounts to the specimen surface in Seemann-Bohlin geometry (right).

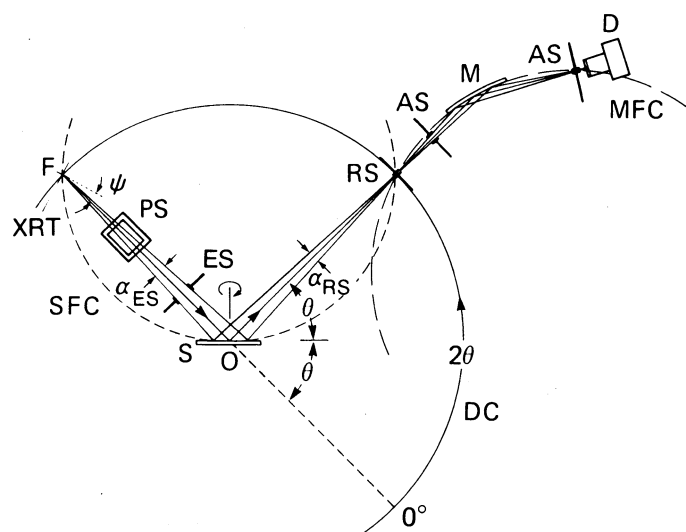


Fig. 2.3.1.3. X-ray optics in the focusing plane of a 'conventional' diffractometer with reflection specimen, diffracted-beam monochromator, and θ - 2θ scanning: ψ take-off angle, DC diffractometer circle, MFC monochromator focusing circle, α_{ES} and α_{RS} entrance- and receiving-slit apertures, θ Bragg angle, 2θ reflection angle, O diffractometer and specimen rotation axis; other symbols listed in Fig. 2.3.1.1.

2.3. POWDER AND RELATED TECHNIQUES: X-RAY TECHNIQUES

$$R_{\text{SFC}} = R_{\text{DC}}/2 \sin \theta. \quad (2.3.1.1)$$

The specimen holder is set parallel to the central ray at 0° and the gears drive the RS-detector arm at twice the speed of the specimen to maintain the θ - 2θ relation at all angles. The source F is the line focus of the X-ray tube viewed at a take-off angle ψ . The actual width, F'_w , is foreshortened to

$$F_w = F'_w \sin \psi. \quad (2.3.1.2)$$

In a typical case, $F'_w = 0.4$ mm and, at $\psi = 5^\circ$, $F_w = 0.03$ mm and the projected angular width is 0.025° for $R = 185$ mm. The angular aperture α_{ES} of the incident beam in the equatorial (focusing) plane is determined by the entrance slit width ES_w (also called the 'divergence slit' since it limits the divergence of the beam) and its distance D_1 from F :

$$\text{ES}_\alpha = 2 \arctan[(\text{ES}_w + F_w)/2D_1]. \quad (2.3.1.3)$$

Because the beam is divergent, the length of specimen irradiated S_l in the direction of the incident beam normal to O varies with θ :

$$S_l = [\alpha(R - D')]/\sin \theta, \quad (2.3.1.4)$$

where α is in radians and D' is the distance from F to the crossover point before ES and is given by $F_w D_1 / (F_w + \text{ES})$. The approximate relation

$$S_l = \alpha R / \sin \theta \quad (2.3.1.5)$$

is close enough for practical purposes (Parrish, Mack & Taylor, 1966). The intensity is nearly proportional to ES_α but the maximum aperture that can be used is determined by S_l and the smallest angle to be scanned $2\theta_{\text{min}}$, as shown in Fig. 2.3.1.4. The entrance-slit width may be increased to obtain higher intensity at the upper angular range; for example, $\text{ES} = 1^\circ$ for the forward-reflection region and 4° for back-reflection.

Some slit designs are shown in Fig. 2.3.1.5. The base is machined with a pair of rectangular shoulders whose separation A is the sum of the diameters of the two rods (a) or bar widths (b) and the central spacers on both ends that determine the slit opening. The distance P between the centre of the slit opening and the edge of the slit frame is kept constant for all slits to avoid angular errors when changing slits. The rods may be molybdenum or other highly absorbing metal and are cemented in

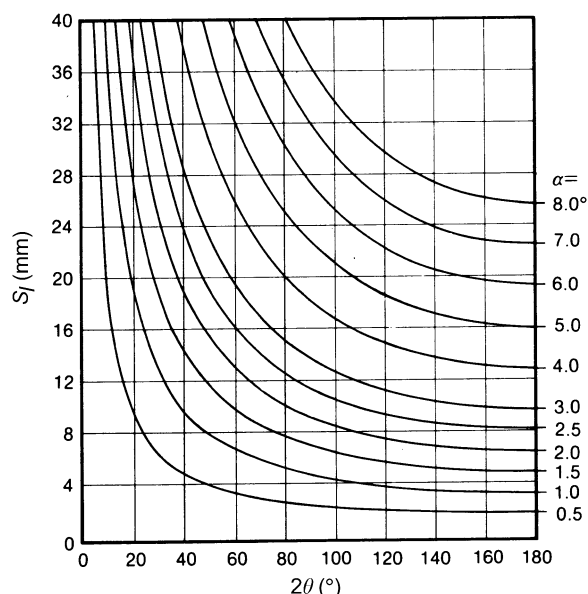


Fig. 2.3.1.4. Length of specimen irradiated, S_l , as a function of 2θ for various angular apertures. $S_l = \alpha R / \sin \theta$, $R = 185$ mm.

place. It may also be made in one piece (c) using machinable tungsten (Parrish & Vajda, 1966).

A variable ES whose width increases with 2θ so that the irradiated length is about the same at all angles has been described by Jenkins & Paolini (1974). It is called a θ -compensating slit in which a pair of semicircular cylinders with a fixed opening is rotated around the axis of the opening by a linkage attached to the specimen shaft of the diffractometer to vary the aperture continuously with θ . The observed intensities must be corrected to obtain the relative intensities and the angular dependence of the aberrations is different from the fixed aperture slit.

Another way to irradiate constantly the entire specimen length is to use a self-centring slit which acts as an entrance and antiscatter slit (de Wolff, 1957). A 1 mm thick brass plate with rounded edge is mounted above the centre of the specimen and is moved in a plane normal to the specimen surface so that the aperture is proportional to $\sin \theta$. It can only be used for forward reflections.

Owing to the beam divergence, the geometric centre of the irradiated specimen length shifts a small amount during the scan (see also §2.3.5.1.5). It is generally advisable to centre the beam at the smallest 2θ to be scanned. Below about 20° , the irradiated length increases rapidly and it is essential to use small apertures and to align the entrance and antiscatter slits carefully. Failure to do this correctly could cause (a) errors in the relative intensities owing to the primary beam exceeding the specimen area, (b) cutoff by the walls of the specimen holder for low-absorbing thick specimens, and (c) increased background from scattering by the specimen holder or the primary beam entering the detector. The transmission specimen method (Subsection 2.3.1.2) has advantages in measuring large d 's.

The beam converges after reflection on the receiving slit RS, whose width defines the reflection and profile width. Only those rays that are within the θ - 2θ setting are in sharp convergence, *i.e.* 'in focus'. The reflections become broader with increasing distance from the RS, and, therefore, this method is not suited for position-sensitive detectors. The RS aperture

$$\alpha_{\text{RS}} = 2 \arctan(\text{RS}_w/2R) \quad (2.3.1.6)$$

is the dominant factor in determining the intensity and resolution. For $\text{RS}_w = 0.1$ mm and $R = 185$ mm, $\alpha_{\text{RS}} = 0.031^\circ$.

Antiscatter slits AS are slightly wider than the beam and are essential in this and other geometries to make certain the detector

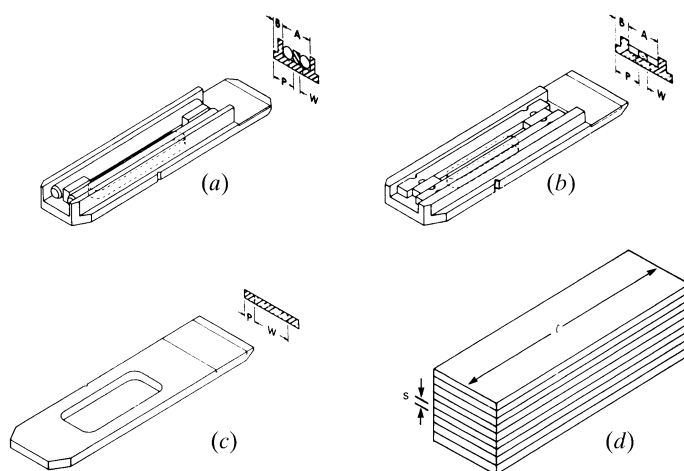


Fig. 2.3.1.5. Slit designs made with (a) rods, (b) bars, and (c) machined from single piece. (d) Parallel (Soller) slits made with spacers or slots cut into the two side pieces (not shown) to position the foils.

2. DIFFRACTION GEOMETRY AND ITS PRACTICAL REALIZATION

can receive X-rays only from the specimen area. They must be carefully aligned to avoid touching the beam.

The use of the long X-ray source makes it necessary to reduce the axial divergence, which would cause very large asymmetry. This is done with two sets of thin (25 to 50 μm) parallel metallic foils PS ('Soller slits'; Soller, 1924) placed before and after the specimen. If a monochromator is used, the set on the side of the monochromator is not essential because the crystal reduces the divergence. The angular aperture of a set of slits is

$$\delta = 2 \arctan(\text{spacing/length}). \quad (2.3.1.7)$$

The overall width of the set and δ determine the width of the specimen irradiated in the axial direction, which remains constant at all 2θ 's. The construction is illustrated in Fig. 2.3.1.5(d). The aperture δ is usually 2 to 5° . Each set of parallel slits reduces the intensity; for example, with 12.5 mm long foils with 1 mm spacings, the intensity is about one-half of that without the parallel slits. The aperture can be selected with any combination of spacings and lengths but the greater the length, the fewer foils are needed, and the less is the intensity loss due to thickness of the metal foils (usually 0.025 mm). These slits can be made as interchangeable units of different apertures.

2.3.1.1.2. Use of monochromators

Many diffractometers are equipped with a curved highly-oriented pyrolytic graphite monochromator placed after the receiving slit as shown in Fig. 2.3.1.3. Although graphite has a large mosaic spread (~ 0.35 to 0.6°), the diffracted beam from the specimen is defined by the receiving slit, which determines the profile shape and width rather than the monochromator. The same results are obtained whether the monochromator is set in the parallel or antiparallel position with respect to the specimen. The most important advantage of graphite is its high reflectivity, which is about 25–50% for Cu $K\alpha$. This is much higher than LiF, Si or quartz monochromators that have been used for powder diffraction. The $K\beta$ filter and the parallel slits in the diffracted beam can be eliminated and, since each reduces the $K\alpha$ intensity by about a factor of two, the use of a graphite monochromator actually increases the available intensity. The diffracted-beam monochromator eliminates specimen fluorescence and the scattered background whose wavelengths are different from that of the monochromator setting. For example, a Cu tube can be used for specimens containing Co, Fe, or other elements with absorption edges at longer wavelengths than Cu $K\alpha$ to produce patterns with low background. Several monochromator geometries are described by Lang (1956).

A specimen in the reflection mode may be used with an incident-beam monochromator and θ - 2θ scanning as shown in Fig. 2.3.1.1(c). One of the principal advantages is that it is possible to adjust the monochromator and slits to remove the $K\alpha_2$ component and produce patterns with only $K\alpha_1$ peaks. The profile symmetry, resolution and instrument function are thus greatly improved; see, for example, Warren (1969), Wölfel (1981), Göbel (1982) and Louër & Langford (1988). The high-quality crystal required causes a large loss of intensity and reduces specimen fluorescence but does not eliminate it. However, Soller slits in the incident beam and a β filter are no longer required and the net loss of intensity can be as low as 20%. Such monochromators can now be provided as standard by diffractometer manufacturers and their use is increasing, but they are not as widely used as the diffracted-beam monochromator.

2.3.1.1.3. Alignment and angular calibration

It is essential to align and calibrate the diffractometer properly. Failure to do so degrades the performance of the instrument, leading to a loss of intensity and resolution, increased background, incorrect profile shapes, and errors that cannot be readily diagnosed. Procedures and devices for this purpose are often provided by the manufacturer. The principles and mechanical devices to aid in making a proper alignment have been described by Parrish & Lowitzsch (1959) and the general procedure by Klug & Alexander (1974, p. 280).

The alignment requires setting the diffractometer axis of rotation to the selected X-ray tube take-off angle at a distance equal to the radius of the diffractometer. The long axes of the X-ray tube focal line, entrance, receiving, and antiscatter slits must be centred, be parallel to the axis of rotation, and lie in the same plane when the instrument is at 0° . The slits are made parallel to the axis of rotation in the manufacture of the diffractometer, and these steps require positioning of the instrument with respect to the line focus. The parallel-slit foils must also be normal to the rotation axis. A flat fluorescent screen made as a specimen to fit into the diffractometer specimen post is used to centre the primary beam by small movements of the ES and/or diffractometer. The diffracted beam can be centred on the curved monochromator with a narrow slit placed at the centre of the monochromator position (with the monochromator removed). The detector arm is then moved to the highest intensity. The procedure is repeated with the receiving slit in position. This is very close to the 0° position described below.

The angular calibration of the diffractometer is usually made by accurately measuring the 0° position to establish a fiducial point. It assumes that the gear system is accurate and that the receiving-slit arm moves exactly to the angle indicated on the scale at all 2θ positions. The determination of the angular precision of the gear train requires special equipment and methods; see, for example, Jenkins & Schreiner (1986). It is

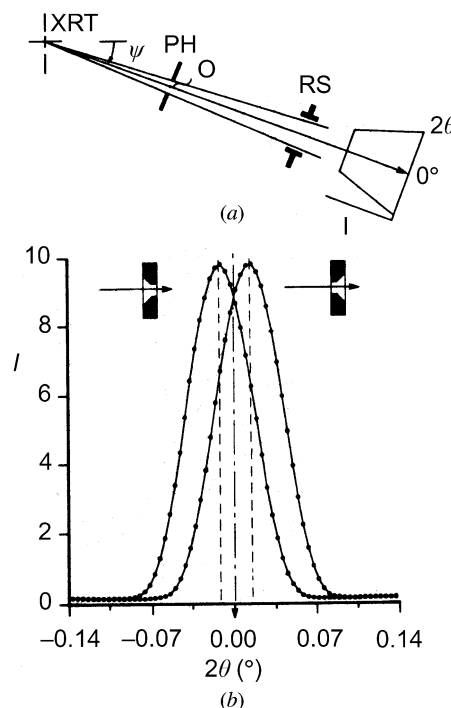


Fig. 2.3.1.6. Zero-angle calibration. (a) XRT X-ray tube anode, ψ take-off angle, O axis of rotation, PH pinhole, RS receiving slit. Intensity distribution at right. (b) 0° position is median of two curves recorded with 180° rotation of PH.

2.3. POWDER AND RELATED TECHNIQUES: X-RAY TECHNIQUES

essential that the setting of the worm against the gear wheel be adjusted for smooth operation. In practice, this is a compromise between minimum backlash and jerky movement. The backlash can be avoided by scanning in the same direction and running the diffractometer beyond the starting angle before beginning the data collection. Incremental angle encoders have been used when very high precision is required.

The 0° position of the diffractometer scale, $2\theta_0$, can be determined with a pinhole placed in the specimen post as shown in Fig. 2.3.1.6(a) (Parrish & Lowitzsch, 1959). The receiving slit is step scanned in 0.01° or smaller increments and the midpoints of chords at various heights are used to determine the angle. To avoid mis-centring errors of the pin-hole, two measurements are made with the specimen post rotated 180° between measurements. The median angle of the two plots is the 0° position as shown in Fig. 2.3.1.6(b) and the diffractometer scale is then reset to this position. The shape of the curves is determined by the relative sizes of the pinhole and the receiving-slit width. With care, the position can be located to about 0.001° . The $2\theta_0$ position can be corrected by using it as a variable in the least-squares refinement of the lattice parameter of a standard specimen.

Another method measures the peak angles of a number of reflections on both sides of 0° , which is equivalent to measuring 4θ . This method may be mechanically impossible with some diffractometers.

The θ - 2θ setting of the specimen post is made with the diffractometer locked in the predetermined 0° position and manually (or with a stepping motor) rotating the post to the maximum intensity. A flat plate can be used as illustrated in Fig. 2.3.1.7(a). The setting can be made to a small fraction of a degree. Fig. 2.3.1.7(b) shows the effect of incorrect θ - 2θ setting, which combines with the flat-specimen aberration to cause a marked broadening and decrease of peak height but no apparent shift in peak position (Parrish, 1958). The effect increases with decreasing θ and could cause systematic errors in the peak intensities as well as incorrect profile broadening.

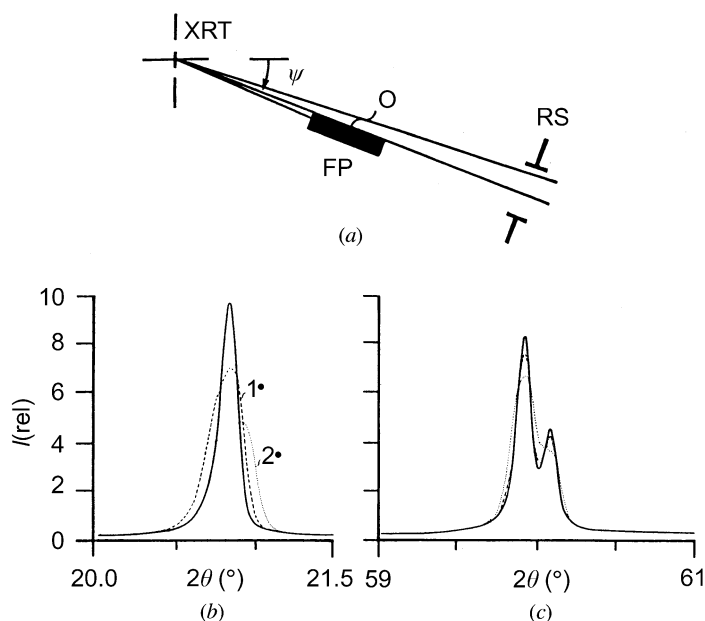


Fig. 2.3.1.7. (a) θ - 2θ setting at 0° . Flat plate or long narrow slit is rotated to position of highest intensity. (b) and (c) Profiles obtained with correct θ - 2θ setting (solid profile) and 1 and 2° mis-settings (dashed profiles) at (b) 21° and (c) 60° (2θ).

2.3.1.1.4. Instrument broadening and aberrations

The asymmetric form, broadening and angular shifts of the recorded profiles arise from the $K\alpha$ doublet and geometrical aberrations inherent in the imperfect focusing of the particular diffractometer method used. There are additional causes of distortions such as the time constant and scanning speed in rate-meter strip-chart recording, small crystallite size, strain, disorder stacking and similar properties of the specimen, and very small effects due to refractive index and related physical aberrations.

Perfect focusing in the sense of reflection from a mirror is never realized in powder diffractometry. The focusing is approximate (sometimes called 'parafocusing') and the practical selection of the instrument geometry and slit sizes is a compromise between intensity, resolution, and profile shape. Increasing the resolution causes a loss of intensity. When setting up a diffractometer, the effects of the various instrument and specimen factors should be taken into account as well as the required precision of the results so that they can be matched. There is no advantage in using high resolution, which increases the recording time (because of the lower intensity and smaller step increments), if the analysis does not require it. A set of runs to determine the best experimental conditions using the following descriptions as a guide should be helpful in obtaining the most useful results.

In the symmetrical geometries where the incident and reflected beams make the same angle with the specimen surface, the effect of absorption on the intensity is independent of the θ angle. This is an important advantage since the relative intensities can be compared directly without corrections. The actual intensities depend on the type of specimen. For a solid block of the material, or a compacted powder specimen, the intensity is proportional to μ^{-1} , where μ is the linear absorption coefficient of the material. The transparency aberration [equation (2.3.1.13)], however, depends on the effective absorption coefficient of the composite specimen.

The need to correct the experimental data for the various aberrations depends on the nature of the required analysis. For example, simple phase identifications can often be made using data in which the uncertainty of the lattice spacing $\Delta d/d$ is of the order of $1/1000$, corresponding to about 0.025 to 0.05° precision in the useful identification range. This is readily attainable in routine practice if care is taken to minimize specimen displacement and the zero-angle calibration is properly carried out. The experimental data can then be used directly for peak search (Subsection 2.3.3.7) to determine the peak angles and intensities (Subsection 2.3.3.5) and the data entered in the search/match program for phase identification.

However, in many of the more advanced aspects of powder diffraction, as in crystal-structure determination and the characterization of materials for solid-state studies, much more detailed and more precise data are required, and this involves attention to the profile shapes. The following sections describe the origin of the instrumental factors that contribute to the shapes and shift the peaks from their correct positions. Many of these factors can be handled individually. With the use of computer programs, they can be determined collectively by using a standard sample without profile broadening and profile-fitting methods to determine the shapes (Subsection 2.3.3.6). The resulting instrument function can then be stored and used to determine the contribution of the specimen to the observed profiles.

A series of papers describing the geometrical and physical aberrations occurring in powder diffractometry has been

2. DIFFRACTION GEOMETRY AND ITS PRACTICAL REALIZATION

published by Wilson (1963, 1974). His work provides the mathematical foundation for understanding the origin and treatment of the various sources of errors. The major aberrations are described in the following and are illustrated with experimental profiles and plots of computed data for better visualization and interpretation of the effects. The information can be used to correct the experimental data, interpret the profile broadening and shifts, and evaluate the precision of the analysis. Chapter 5.2 contains tables listing the centroid displacements and variances of the various aberrations.

The magnitudes of the aberrations and their effects are illustrated in Figs. 2.3.1.8(a) and (b), which show the Cu $K\alpha_1, K\alpha_2$ spectrum inside the experimental profile. At high 2θ 's, the shape of the experimental profile is largely determined by the spectral distribution, but at low 2θ 's the aberrations are the principal contributors. The basic experimental high-resolution profile shapes from specimens without appreciable broadening effects (NIST silicon powder standard) are shown in Figs. 2.3.1.8(c)–(f). The solid-line profiles were obtained with a reflection specimen (Fig. 2.3.1.3), and the dashed-line profiles with transmission-specimen geometry (Fig. 2.3.1.12). The differences in the $K\alpha_1, K\alpha_2$ doublet separations are explained in Subsection 2.3.1.2. These profiles are the basic instrument functions which show the profile shapes contained in all

reflections recorded with these methods. The shapes are modified by changing slit sizes.

2.3.1.1.5. Focal line and receiving-slit widths

The projected source width F_w and receiving-slit width RS_w each add a symmetrical broadening to the profiles that is constant for all angles. Both the profile width and the intensity increase with increasing take-off angle (Section 2.3.5). However, the contribution of F_w is small when the line focus is used, Fig. 2.3.1.9(a). The receiving slit can easily be changed and it is one of the most important elements in controlling the profile width, intensity, and peak-to-background ratio, as is shown in Figs. 2.3.1.9(a) and (c). Because of the contributions of other broadening factors, α_{RS} can be about twice α_F (line focus) without significant loss of resolution.

The projected width of the X-ray tube focus F_w is given in equation (2.3.1.2). The aperture is

$$\alpha_F = 2 \arctan(F_w/2R). \quad (2.3.1.8)$$

For a line focus with actual width $F'_w = 1$ mm, $\psi = 5^\circ$, and $R = 185$ mm, $\alpha_F = 0.011^\circ$. The receiving-slit aperture is

$$\alpha_{RS} = 2 \arctan(RS_w/2R). \quad (2.3.1.9)$$

For $RS_w = 0.2$ mm and $R = 185$ mm, α_{RS} is 0.062° . The FWHM of the profiles is always greater than the receiving-slit aperture because of the other broadening factors.

2.3.1.1.6. Aberrations related to the specimen

The major displacement errors arising from the specimen are (1) displacement of the specimen surface from the axis of rotation, (2) use of a flat rather than a curved specimen, and (3) specimen transparency. These are illustrated schematically for the focusing plane in Fig. 2.3.1.10(a). The rays from a highly absorbing or very thin specimen with the same curvature as the focusing circle converge at A without broadening and at the correct 2θ . The rays from the flat surface cause an asymmetric profile shifted to B . Penetration of the beam below the surface combined with the flat specimen causes additional broadening and a shift to C .

The most frequent and usually the largest source of angular errors arises from displacement of the specimen surface from the diffractometer axis of rotation. It is not easy to avoid and may arise from several sources. It is advisable to check the reproducibility of inserting the specimen in the diffractometer by recording an isolated peak at low 2θ for each insertion. If only a radial displacement s occurs, the reflection is shifted

$$\Delta 2\theta(\text{rad}) = \pm 2s \cos \theta / R, \quad (2.3.1.10)$$

where R is the diffractometer radius. A plot of equation (2.3.1.10) is shown in Fig. 2.3.1.10(b). The shift is to larger or smaller angles depending on the direction of the displacement and there is no broadening if the displacement is only radial and relatively small. Even a small displacement causes a relatively large shift; for example, if $s = +0.1$ mm and $R = 185$ mm, $\Delta 2\theta = +0.06^\circ$ at $20^\circ 2\theta$. This gives rise to a systematic error in the recorded reflection angles, which increases with decreasing 2θ . It could be handled with a $\cos \theta \cot \theta$ plot, providing it was the only source of error. There are other possible sources of displacement such as (a) if the bearing surface of the specimen post was not machined to lie exactly on the axis of rotation, (b) improper specimen preparation or insertion in which the surface was not exactly coincident with the bearing surface or (c) nonplanar specimen surface, irregularities, large particle sizes, and specimen transparency. Source (a) leads to a constant error

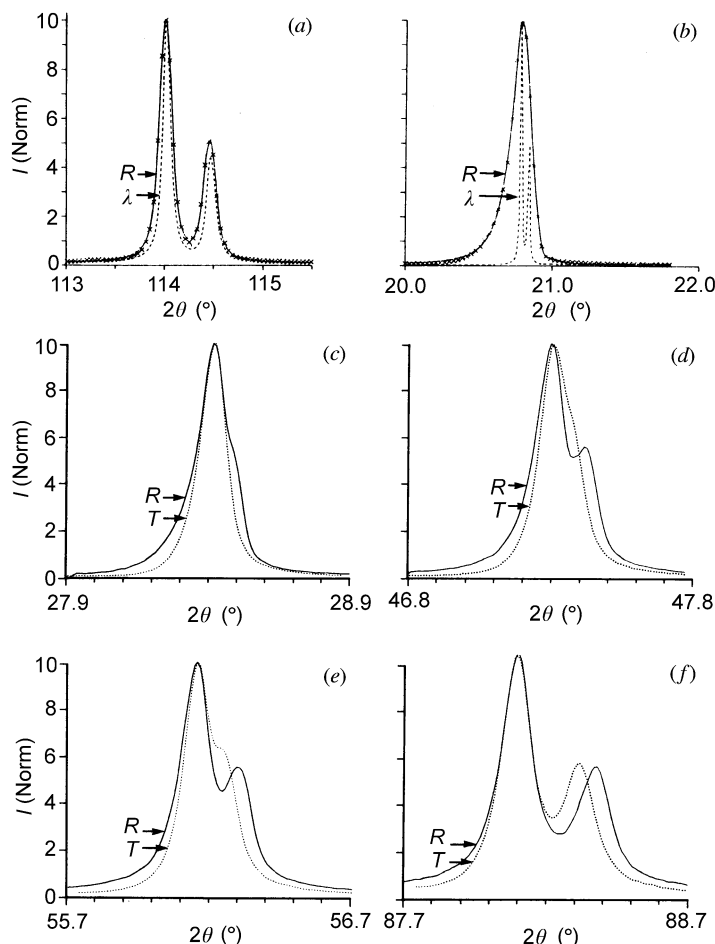


Fig. 2.3.1.8. Diffractometer profiles. (a) and (b) Spectral profiles λ of Cu $K\alpha$ doublet (dashed-line profiles) inside experimental profiles R (solid line). (c)–(f) Experimental profiles with reflection specimen (R) geometry (Fig. 2.3.1.3) with $\alpha_{ES} 1^\circ$ and $\alpha_{RS} 0.046^\circ$ (solid line profiles), and transmission specimen (T) (Fig. 2.3.1.12) with $\alpha_{ES} 2^\circ$ and receiving axial divergence parallel slits (dotted profiles). Cu $K\alpha$ radiation. (a) Si(531), (b) quartz(100), (c) Si(111), (d) Si(220), (e) Si(311), and (f) Si(422).

2.3. POWDER AND RELATED TECHNIQUES: X-RAY TECHNIQUES

in all measurements, and errors due to (b) and (c) vary with each specimen.

Ideally, the specimen should be in the form of a focusing torus because of the beam divergence in the equatorial and axial planes. The curvatures would have to vary continuously and differently during the scan and it is impracticable to make specimens in such forms. An approximation is to make the specimen in a flexible cylindrical form with the radius of curvature increasing with decreasing 2θ (Ogilvie, 1963). This requires a very thin specimen (thus reducing the intensity) to avoid cracking and surface irregularities, and also introduces background from the substrate. A compromise uses rigid curved specimens, which match the SFC (Fig. 2.3.1.3) at the smallest 2θ angle to be scanned, and this eliminates most of the aberration (Parrish, 1968). A major disadvantage of the curvature is that it is not possible to spin the specimen.

In practice, a flat specimen is almost always used. The specimen surface departs from the focusing circle by an amount h at a distance $l/2$ from the specimen centre:

$$h = R_{FC} - [R_{FC}^2 - (l^2/2)]^{1/2}. \quad (2.3.1.11)$$

This causes a broadening of the low- 2θ side of the profile and shifts the centroid $\Delta 2\theta$ to lower 2θ :

$$\Delta 2\theta(\text{rad}) = -\alpha^2/(6 \tan \theta). \quad (2.3.1.12)$$

For $\alpha = 1^\circ$ and $2\theta = 20^\circ$, $\Delta 2\theta = -0.016^\circ$. The peak shift is about one-third as large as the centroid shift in the forward-reflection region. This aberration can be interpreted as a continuous series of specimen-surface displacements, which increase from 0 at the centre of the specimen to a maximum value at the ends. The effect increases with α and decreasing 2θ . The profile distortion is magnified in the small 2θ -angle region where the axial divergence also increases and causes similar effects. Typical flat-specimen profiles are shown in Fig. 2.3.1.10(c) and computed centroid shifts in Fig. 2.3.1.10(d).

The specimen-transparency aberration is caused by diffraction from below the surface of the specimen which asymmetrically

broadens the profile (Langford & Wilson, 1962). The peak and centroid are shifted to smaller 2θ as shown in Fig. 2.3.1.10(e). For the case of a thick absorbing specimen, the centroid is shifted

$$\Delta 2\theta(\text{rad}) = \sin 2\theta/2\mu R \quad (2.3.1.13)$$

and for a thin low-absorbing specimen

$$\Delta 2\theta(\text{rad}) = t \cos \theta/R, \quad (2.3.1.14)$$

where μ is the effective linear absorption coefficient of the specimen used, t the thickness in cm, and R the diffractometer radius in cm. The intermediate absorption case is described by Wilson (1963). A plot of equation (2.3.1.13) for various values of μ is given in Fig. 2.3.1.10(f). The effect varies with $\sin 2\theta$ and is maximum at 90° and zero at 0° and 180° . For example, if $\mu = 50 \text{ cm}^{-1}$, the centroid shift is -0.033° at 90° and falls to -0.012° at $20^\circ 2\theta$.

The observed intensity is reduced by absorption of the incident and diffracted beams in the specimen. The intensity loss is $\exp(-2\mu/x_s \text{ cosec } \theta)$, where μ is the linear absorption coefficient of the powder sample (it is almost always smaller than the solid material) and x_s is the distance below the surface, which may be equal to the thickness in the case of a thin film or low-absorbing material specimen. The thick (1 mm) specimen of LiF in Fig. 2.3.1.10(e) had twice the peak intensity of the thin (0.1 mm) specimen.

The aberration can be avoided by making the sample thin. However, the amount of incident-beam intensity contributing to the reflections could then vary with θ because different amounts are transmitted through the sample and this may require corrections of the experimental data. Because the effective reflecting volume of low-absorbing specimens lies below the surface, care must be taken to avoid blocking part of the diffracted beam with the antiscatter slits or the specimen holder, particularly at small 2θ .

There are additional problems related to the specimen such as preferred orientation, particle size, and other factors; these are discussed in Section 2.3.3.

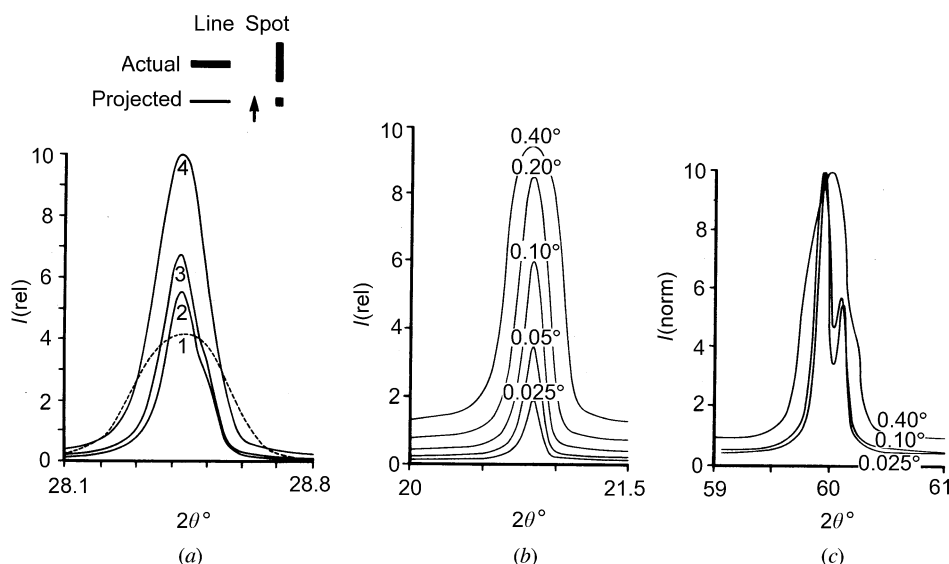


Fig. 2.3.1.9. (a) Effect of source size on profile shape, Cu $K\alpha$, $\alpha_{ES} 1^\circ$, $\alpha_{RS} 0.05^\circ$, Si(111).

No.	Projected size (mm)	FWHM ($^\circ 2\theta$)
1	1.6×1.0 (spot)	0.31
2	0.32×10 (line)	0.11
3	0.16×10 (line)	0.13
4	0.32×12 (line)	0.17

Effect of receiving-slit aperture α_{RS} on profiles of quartz (b) (100) and (c) (121); peak intensities normalized, Cu $K\alpha$, $\alpha_{ES} 1^\circ$.

2. DIFFRACTION GEOMETRY AND ITS PRACTICAL REALIZATION

2.3.1.1.7. Axial divergence

Divergence in the axial direction (formerly also called 'vertical divergence') causes asymmetric broadening and shifts the reflections. The aberration is illustrated in Fig. 2.3.1.11 for a low- 2θ reflection in the transmission-specimen mode (Subsection 2.3.1.2). The narrow profile was obtained with $\delta = 4.4^\circ$ parallel slits placed between the monochromator and detector, and the broad profile with the slits removed. The slits caused a 33% reduction in peak intensity. This problem was recognized in the first design of the diffractometer using the X-ray tube line focus when parallel slits were used in the incident and diffracted beams to limit the effect (Parrish, 1949). Increasing the radius reduces the effect if the slit length is kept constant. The intensity is also

reduced because the chord length intercepted is a smaller fraction of the longer radius diffraction cone. The construction of parallel (Soller) slits (Soller, 1924) is shown in Fig. 2.3.1.5(d).

The calculation of the aberration and the present status is summarized by Wilson (1963, pp. 40–45). The results depend on the aperture of the parallel slits, the length of the entrance and receiving slits, and 2θ . In the limit of small s , the shift of the centroid is

$$\Delta(2\theta, \text{rad}) = (s/l)^2 \cot 2\theta/6, \quad (2.3.1.15)$$

where s is the spacing and l the length of the foils. The shift becomes very large at small 2θ 's but not infinite as equation (2.3.1.15) implies. The shift is to smaller 2θ 's in the forward-reflection region and to larger 2θ 's in back-reflection. However, the mathematical formulation is difficult to quantify because in the forward-reflection region the axial divergence convolves with the flat-specimen aberration to increase the asymmetry. In the back-reflection region, the effect is not so obvious because the distortion is smaller and the Lorentz and dispersion factors also stretch the profiles to higher angles.

2.3.1.1.8. Combined aberrations

Additional aberrations are caused by inaccurate instrument set-up and alignment. For example, if the receiving-slit position is incorrect, the profiles are broadened. If, in addition, the incident beam is mis-centred or the θ - 2θ is incorrect, a peak shift accompanies the broadening because the aberrations convolute, causing larger distortions and peak shifts than the individual aberrations, for example, flat-specimen, transparency, and axial divergence.

2.3.1.2. Transmission specimen, θ - 2θ scan

Transmission-specimen methods are not as widely used as reflection methods but they provide important supplemental data and have advantages in a number of applications. Reflections occur from lattice planes oriented normal to the specimen surface rather than parallel. Reflection and transmission patterns can be compared to determine texture and preferred-orientation effects. The transmission method is better suited to the measurement of large d 's. Smaller specimen volumes are required. The surface 'roughness' which may cause large intensity errors due to the microabsorption in reflection specimens is largely reduced.

The same basic diffractometer is used for both methods but the geometry is different because the diffracted beam continues to

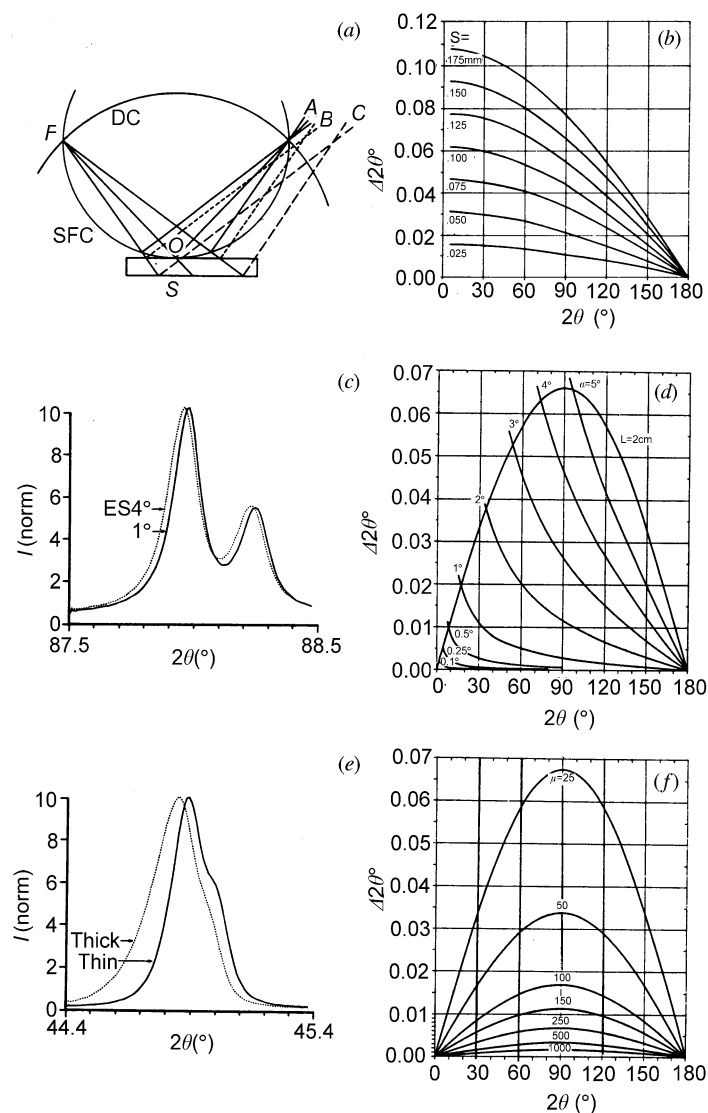


Fig. 2.3.1.10. (a) Origin of specimen-related aberrations in focusing plane of conventional reflection specimen diffractometer (Fig. 2.3.1.3). A no aberration from curved specimen; B flat specimen; C specimen displacement from 0. (b) Computed angular shifts caused by specimen displacement, $R = 185$ mm. (c) Flat-specimen asymmetric aberration, Si(422), Cu $K\alpha_1$, $K\alpha_2$ peak intensities normalized. (d) Computed flat-specimen centroid shifts for various apertures; parabola for constant irradiated 2 cm specimen length. (e) Transparency asymmetric aberration, LiF(200) powder reflection, Cu $K\alpha$, peak intensities normalized, thin specimen (solid-line profile) 0.1 mm thick; thick specimen (dotted-line profile) 1.0 mm, $\alpha_{ES} 1^\circ$, $\alpha_{RS} 0.046^\circ$. (f) Computed transparency centroid shifts for various values of linear absorption coefficient.

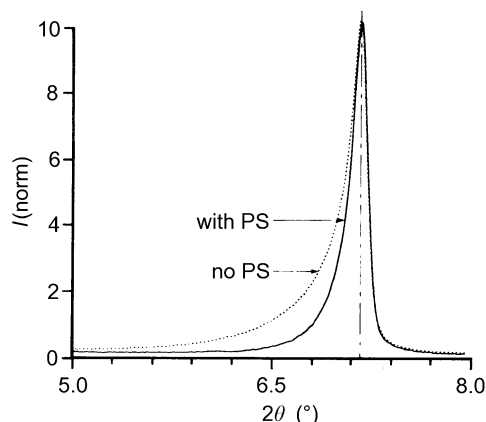
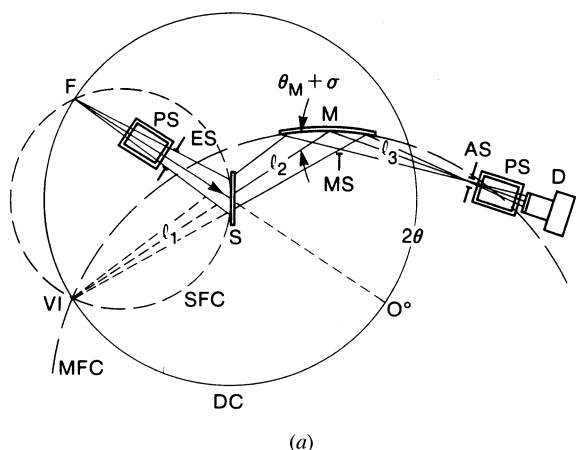


Fig. 2.3.1.11. Effect of axial divergence on profile shape. Narrow profile recorded with parallel slits (PS), $\delta = 4.4^\circ$ between monochromator and detector Fig. (2.3.1.12), and broad profile with these parallel slits removed. Faujasite, Cu $K\alpha$, $\alpha_{ES} 2^\circ$.

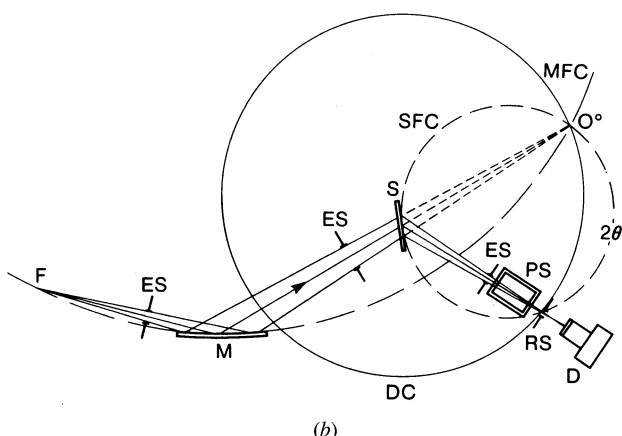
2.3. POWDER AND RELATED TECHNIQUES: X-RAY TECHNIQUES

diverge after it passes through the specimen and the monochromator is required to refocus the beam, on the detector as shown in Fig. 2.3.1.12 (de Wolff, 1968*b*; Parrish, 1958). The monochromator can be placed before or after the specimen and the position has different effects on the pattern. Using the monochromator in the diffracted beam, the intensity and width of the profiles are determined by the X-ray focal line width and the quality of the bent monochromator rather than the receiving slit which serves as an antiscatter slit. This geometrical arrangement places the virtual image VI of the focal line at the intersection of the focusing circles. After reflection from the specimen, the divergent beam is again reflected by the focusing crystal *M* and converges on the detector. The pattern is recorded with θ - 2θ scanning with the monochromator and detector both mounted on a rigid arm rotating around the diffractometer axis. A beam stop MS can be translated and moved in and out near the crossover point to prevent the primary beam from entering the detector at small 2θ 's. To avoid long radii, the crystal surface is cut at an angle σ (about 3°) to the reflecting lattice plane. The distances are related by

$$\begin{aligned} (l_1 + l_2)/l_3 &= [\sin(\theta_M + \sigma)]/[\sin(\theta_M - \sigma)] \\ R_{FC} &= [l_1 + l_2]/[2 \sin(\theta_M + \sigma)] \\ &= l_3/[2 \sin(\theta_M - \sigma)], \end{aligned} \quad (2.3.1.16)$$



(a)



(b)

Fig. 2.3.1.12. X-ray optics of the transmission specimen with asymmetric focusing monochromator and θ - 2θ scanning. (a) Monochromator in diffracted beam. θ_M Bragg angle of monochromator with surface cut at angle σ to reflecting plane, MS adjustable beam stop, l_1 , l_2 , and l_3 defined in text and other symbols listed in Fig. 2.3.1.3. (b) Monochromator in incident beam, equivalent to Guinier focusing camera.

where θ_M is the Bragg angle of the monochromator for the selected wavelength and the l 's are shown in Fig. 2.3.2.12(a).

Because the profile shape and the intensity are determined by the monochromator, the crystal quality and the accuracy of the bending are crucial factors in determining the quality of the pattern. A flat thin quartz (101) wafer bent with a special device to approximate a section of a logarithmic spiral has been successfully used (de Wolff, 1968*b*). The curvature can be varied to obtain the sharpest focus. Thin silicon crystals that can be bent are now available, and Johann and Johannsen asymmetric crystals may be used. Pyrolytic graphite monochromators are not applicable; the radii would be longer because graphite is too soft to be cut at an angle, and a receiving slit would be necessary to define the diffracted beam because the monochromator produces a broad reflection.

A polarization factor is introduced by the monochromator,

$$p = (1 + k \cos^2 2\theta)/(1 + k), \quad (2.3.1.17)$$

where $k = \cos^2 2\theta_M$ for mosaic crystals and $k = \cos 2\theta_M$ for perfect crystals. The value of k is strongly dependent on the surface finish of the crystal and the crystal should be measured to determine the effect. A specimen with accurately known structure factors such as silicon can be used to calibrate the intensities.

The $K\alpha$ -doublet separation is zero at the 2θ angle at which the dispersion of the specimen compensates that of the monochromator, *i.e.* the 2θ at which the monochromator is aligned and also depends on the distances. The $K\alpha_1$ and $K\alpha_2$ peaks are superposed and appear as a single peak over a small range of 2θ 's. The $K\alpha_2$ peak gradually separates with increasing 2θ but the separation is less than calculated from the wavelengths and the intensity ratio may not be 2:1 until higher angles are reached as shown in Fig. 2.3.1.8.

A larger angular aperture α_T can be used for transmission than for reflection α_R because the specimen is more nearly normal to than parallel to the primary beam:

$$\alpha_T/\alpha_R = 2R_D/[1 + (R_D/l_2)L_S], \quad (2.3.1.18)$$

where the diffractometer radius $R_D = l_1$. For $R_D = 170$ mm, specimen length $L_S = 20$ mm and $l_2 = 65$ mm; α_T could be 4.7 times larger than α_R but the monochromator length usually limits it to about 3° . The smallest reflection angle that can be measured is

$$2\theta_{\min} = \alpha_T[(R_D + l_2)/l_2]. \quad (2.3.1.19)$$

Using $\alpha_T = 0.5^\circ$, $2\theta_{\min} = 1.75^\circ$ and $d = 50 \text{ \AA}$ for Cu $K\alpha$ radiation.

Specimen preparation is not difficult and the preparation can be easily tested and changed. The specimen must be X-ray transparent and can be a free-standing film or foil, or a powder cemented to a thin substrate. The substrate selection is important because its pattern is included. If both transmission and reflection patterns are to be compared, the substrate should be selected to have a minimal contribution to both. For example, Mylar is a good substrate for transmission but has a strong reflection pattern, and although rolled Be foil has a few reflections it is often satisfactory for both.

The absorption factor is

$$A = (t/\cos \theta) \exp(-s/\cos \theta), \quad (2.3.1.20)$$

where t is the powder thickness and s is the sum of the products of the absorption coefficients and thicknesses of the powder and the substrate. The optimum specimen thickness to give the highest intensity is $\mu t = 1$, *i.e.* the specimen should transmit about 38% of the incident $K\alpha$ intensity. The transmission can be

2. DIFFRACTION GEOMETRY AND ITS PRACTICAL REALIZATION

easily measured with a standard specimen set to reflect the $K\alpha$ and the specimen to be measured inserted normal to the diffracted beam in front of the detector. It is not critical to achieve the exact value and a range of $\pm 15\text{--}20\%$ of the transmission can be tolerated. This minimizes the effect of the absorption change with 2θ , and corrections of the relative intensities are required only when accurate values are required.

The intensity of the incident beam can be measured at 0° in the same geometry and used to scale the relative intensities to 'absolute' values. The flat specimen, transparency, and specimen surface displacement aberrations are similar to those in reflection specimen geometry except that they vary as $\sin\theta$ rather than $\cos\theta$. This is an important factor in the measurement of large- d -spacing reflections. The flat-specimen effect is smaller because the irradiated specimen length is usually smaller. The transparency error is also usually smaller because thin specimens are used.

An important advantage of the method is that the specimen displacement can be directly determined by measuring the peak in the normal position and again after rotating the specimen holder 180° . The correct peak position is at one-half the angle between the two values. The axial divergence has the same effect as in reflection. The limitations are that only the forward-reflection region is accessible, and the intensity is about one-half of the reflection method (except at small angles) because smaller specimen volumes are used.

An alternative arrangement for the transmission specimen mode is to use an incident-beam monochromator as shown in Fig. 2.3.1.12(b). This is similar to the geometry used in the Guinier powder camera with the detector replacing the film. A high-quality focusing crystal is required. Wölfel (1981) used a symmetrical focusing monochromator with 260 mm focal length for quantitative analysis. Göbel (1982) used an asymmetric monochromator with a position-sensitive detector for high-speed scanning, see §2.3.5.4.1. By proper selection of the source size and distances, the $K\alpha_2$ can be eliminated and the pattern contains only the $K\alpha_1$ peaks (Guinier & Sébilleau, 1952). This geometry can have high resolution with the FWHM typically about 0.05 to 0.07° . The profile widths are narrower for the subtractive setting of the monochromator than for the additive setting.

The pattern is recorded with θ - 2θ scanning. The 0° position can be determined by measuring 4θ , *i.e.* peaks above and below 0° , or calibration can be made with a standard specimen. A slit after the monochromator limits the size of the beam striking the specimen. The width and intensity of the powder reflections are limited by the receiving-slit width. A parallel slit is used between the specimen and detector to limit axial divergence.

The full spectrum from the X-ray tube strikes the monochromator and only the monochromatic beam reaches the specimen, so that it is preferred for radiation-sensitive materials. On the other hand, the radiation reaching the specimen may cause fluorescence (though considerably less than the full spectrum) which adds to the background.

2.3.1.3. Seemann-Bohlin method

The Seemann-Bohlin (*S-B*) diffractometer has the specimen mounted on a radial arm instead of the axis of rotation and a linkage or servomechanism moves the detector around the circumference of a fixed-radius focusing circle while keeping it pointed to the stationary specimen. All reflections occur simultaneously focused on the focusing circle as shown in Fig. 2.3.1.13(a). The method was originally developed for powder cameras by Seemann (1919) and Bohlin (1920) but was not widely used because of the limited angular range and the broad

reflections caused by inclination of the rays to the film. The diffractometer eliminates the broadening and extends the angular range. Diffractometers designed for this geometry have been described by Wassermann & Wiewiorosky (1953), Segmüller (1957), Kunze (1964*a,b*), Parrish, Mack & Vajda (1967), King, Gillham & Huggins (1970), Feder & Berry (1970), and others.

The geometry is shown in Fig. 2.3.1.13(b) (Parrish & Mack, 1967). Reflections occur from lattice planes with varying inclinations β_H to the specimen surface. The reflecting position of a plane H is $\theta_H = \gamma + \beta_H$, where γ is the incidence angle and $4\theta_H$ the reflection angle. The maximum value of β_H is about 45° . It is essential to align the specimen tangent to FC. This is a critical adjustment because even a small misalignment causes profile broadening and loss of peak intensity.

The source may be the line focus of the X-ray tube [F in Fig. 2.3.1.13(b)] or at the focus of a monochromator [ES in Fig. 2.3.1.13(a)]; in the latter case, the entrance slit at F' limits the divergent beam reaching the specimen. The source, specimen centre O , and receiving slit RS lie on the specimen focusing circle SFC, which has a fixed radius r . The incidence angle γ is given by

$$\gamma = \arcsin(b/2r), \quad (2.3.1.21)$$

where b is the distance from F or F' to O , or $2r \sin \gamma$. The γ angle determines the angular range that can be recorded with a given r , decreasing γ decreases $2\theta_{\min}$. The relationships of specimen position on the focusing circle and the recording range

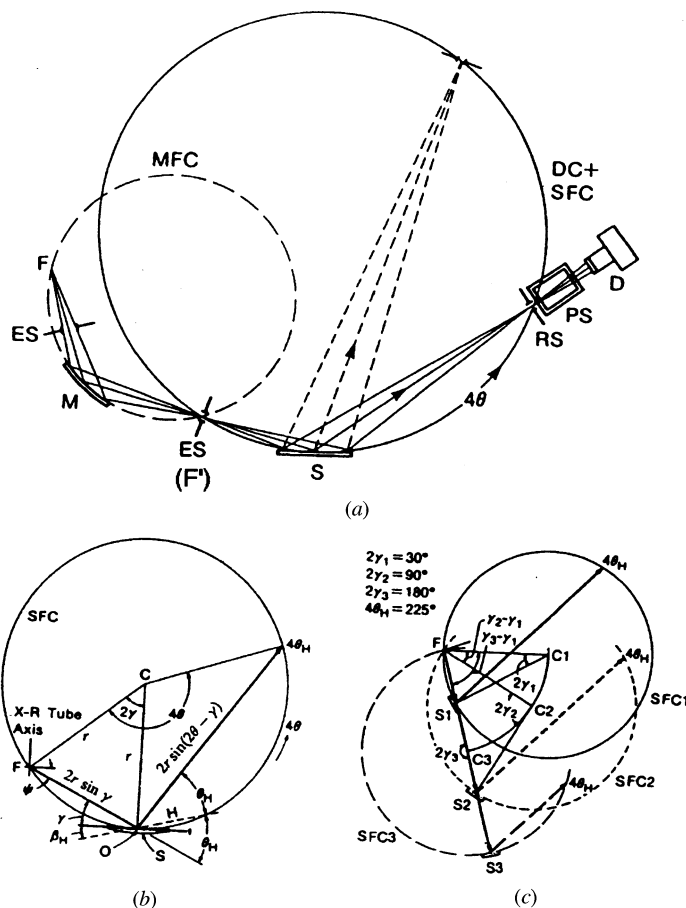


Fig. 2.3.1.13. Seemann-Bohlin method. (a) X-ray optics using incident-beam monochromator. (b) X-ray tube line-focus source showing geometrical relations: γ mean angle of incident beam, β_H inclination of reflecting plane H to specimen surface, θ_H Bragg angle of H plane, t tangent to focusing circle at O . (c) Diffractometer settings for various angular ranges.

2.3. POWDER AND RELATED TECHNIQUES: X-RAY TECHNIQUES

are illustrated in Fig. 2.3.1.13(c). To change the range requires rotation of the X-ray tube axis or the diffractometer around F . The detector must also be repositioned. For forward-reflection measurements, γ is usually $\leq 10^\circ$. Extreme care must be used in the specimen preparation to avoid errors due to microabsorption (particle-shadowing) effects, which increase with decreasing γ . The 0° position cannot be measured directly and a standard is used for calibration. The range from 0° to about $15^\circ 2\theta$ is inaccessible because of mechanical dimensions. At $\gamma = 90^\circ$, only the back-reflection region can be scanned.

The aperture of the beam striking the specimen is

$$\alpha_{SB} = 2 \arctan(ES_w/2a), \quad (2.3.1.22)$$

where ES_w is the entrance slit width and a the distance between F or F' and the slit. The irradiated specimen length l is constant at all angles, $l = 2\alpha r$. A large aperture can be used to increase intensity since the specimen is close to F . However, the selection of α is limited if γ is small, and also because of the large flat-specimen aberration.

The receiving-slit aperture varies with the distance of the slit to the specimen

$$\alpha_{RS}(^\circ 4\theta) = 2 \arctan RS_w/[2r \sin(2\theta - \gamma)]. \quad (2.3.1.23)$$

Consequently, the resolution and relative intensity gradually change across the pattern. The S - B has greater widths at the smaller 2θ 's and nearly the same widths at the higher angles compared with the θ - 2θ diffractometer. The aperture can be kept constant by using a special slit with offset sides (to avoid shadowing) and pointing the opening to C while the detector remains pointed to O (Parrish *et al.*, 1967). The slit opening is tangent to FC and inclined to the beam and rotates while scanning. The constant aperture slit has

$$\alpha_{RS}(^\circ 4\theta) = 2 \arctan(RS_w/2r). \quad (2.3.1.24)$$

The axial divergence is limited by parallel slits as in conventional diffractometry and the effects are about the same. The equatorial aberrations are also similar but larger in magnitude. The specimen-aberration errors are listed in Table 5.2.7.1. The flat specimen causes asymmetric broadening; the shift is proportional to α_{ES}^2 and increases with decreasing θ . It can be eliminated by making the specimen with the same curvature as $r = FC$. In this case, one curvature satisfies the entire angular range because the focusing circle has a fixed radius. However, the curvature precludes rotating the specimen. The specimen transparency also causes asymmetric broadening and a peak shift that increases with decreasing θ . For $\mu h \rightarrow 0$, the geometric term is the same as for specimen displacement (Mack & Parrish, 1967).

The diffracted intensity is proportional to $I_0 A(\mu h) TB$, where I_0 is the incident intensity determined by α , δ , and the axial length L of the incident-beam assembly, $A(\mu h)$ is the specimen absorption factor, T the transmission of the air path, and B the length L_{RS} of the diffracted ring intercepted by the slit. The X-rays reflected at a depth x below the specimen surface are attenuated by

$$\exp\{-[\mu x \operatorname{cosec} \delta + \mu x \operatorname{cosec}(2\theta - \delta)]\}, \quad (2.3.1.25)$$

where μ is the linear absorption coefficient. The asymmetric geometry causes the absorption to vary with the reflection angle. The air absorption path varies with the distance O to RS and reaches a maximum at $180^\circ + 2\gamma$. The expression for air transmission includes the radius of the X-ray tube R_T , which is needed only for the case where the X-ray tube focal line is used as F . In a typical instrument with X-ray tube source F and $r = 174$ mm, the transmission of $\text{Cu } K\alpha$ decreases from 90% at

$40^\circ 4\theta$ to 62% at 210° , and $\text{Cr } K\alpha$ from 73 to 23% at the same angles.

Some of the advantages of the method include the following: (a) the fixed specimen makes it possible to simplify the design of specimen environment devices; (b) a large aperture can be used and the intensities are higher than for conventional diffractometers; (c) the flat-specimen aberration can be eliminated by a single-curvature specimen; (d) a small γ angle can be used to increase the path length l in the specimen, and hence the intensity of low-absorbing thin-film samples ($l = t/\sin \gamma$ and for $\gamma = 5^\circ$, $l = 11.5t$); (e) the method is useful in thin-film and preferred-orientation studies because about a 45° range of lattice-plane orientations can be measured and compared with conventional patterns. The limitations include (a) the more complicated diffractometer and its alignment, (b) limited angular range of about 10 to $110^\circ 2\theta$ for the forward-reflection setting, (c) extreme care required in specimen preparation, and (d) larger aberration errors.

2.3.1.4. Reflection specimen, θ - θ scan

In this geometry, the specimen is fixed in the horizontal plane and the X-ray tube and detector are synchronously scanned in the vertical plane in opposite directions above the centre of the specimen as shown in Fig. 2.3.1.14. The distances source to S and S to RS are equal to that the angles of incidence and diffraction and a constant $d\theta/dt$ are maintained over the entire angular range. A focusing monochromator can be used in the incident or diffracted beam. High- and low-temperature chambers are simplified because the specimen does not move. The arms carrying the X-ray tube and detector must be counterbalanced because of the unequal weights. The method has advantages in certain applications such as the measurement of liquid scattering without a covering window, high-temperature molten samples, and other applications requiring a stationary horizontal sample (Kaplow & Averbach, 1963; Wagner, 1969).

2.3.1.5. Microdiffractometry

There are two types of microdiffraction: (a) only a very small amount of powder is available, and (b) information is required from very small areas of a conventional-size specimen. Small-volume samples have been analysed with a conventional diffractometer by concentrating the powder over a small spot centred on a single-crystal plate such as silicon (510) or an

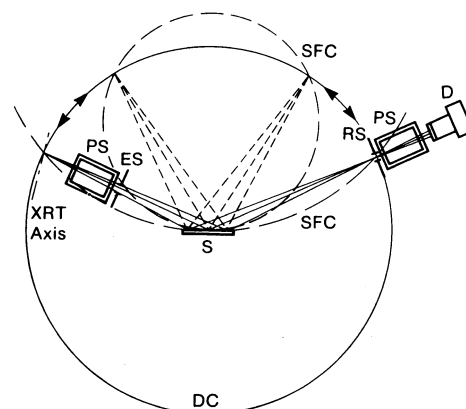


Fig. 2.3.1.14. Optics of θ - θ scanning diffractometer. X-ray tube and detector move synchronously in opposite directions (arrows) around fixed horizontal specimen. A focusing monochromator can be used after the receiving slit.

2. DIFFRACTION GEOMETRY AND ITS PRACTICAL REALIZATION

AT-cut quartz plate, or on Mylar for transmission. It is essential to rotate the specimen and increase the count time. A Gandolfi camera has also been used for very small specimens (see Section 2.3.4). A high-brilliance microfocus X-ray source has been used with a collimator made of 10 to 100 μm internal-diameter capillary tube. An X-Y stage is used with an optical microscope to locate selected areas of the specimen.

A microdiffractometer has been designed for microanalysis, Fig. 2.3.1.15 (Rigaku Corporation, 1990). It has been used to determine phases and stress in areas $< 10^4 \mu\text{m}^2$ (Goldsmith & Walker, 1984). The key to the method is the use of an annular-ring receiving slit, which transmits the entire diffraction cone to the detector instead of a small chord as in conventional diffractometry, thereby utilizing all the available intensity. The pattern is scanned by translating the ring and detector along the direct-beam path so that

$$2\theta = \arctan(R_{\text{RS}}/L), \quad (2.3.1.26)$$

where R_{RS} is the radius of the ring slit and L the distance from the fixed specimen. For $R_{\text{RS}} = 15 \text{ mm}$, L varies from 171 to 9 mm in the transmission range 5 to $60^\circ 2\theta$; a 50 mm diameter scintillation counter is used. A doughnut-shaped proportional counter (3/4 of a full circle) is used for the 30 to 150° reflection specimen mode. The slit width is 0.2 mm and the aperture varies with 2θ . The intensities fall off at the higher 2θ 's because of the small incidence angles to the slit. An alternative method uses a position-sensitive proportional counter. Steinmeyer (1986) has described applications of microdiffractometry.

By using synchrotron radiation (Section 2.3.2), single-crystal data for structure determination can now be obtained from a microcrystal about 5–10 μm in size; see Andrews *et al.* (1988), Bachmann, Kohler, Schultz & Weber (1985), Harding (1988), Newsam, King & Liang (1989), Cheetham, Harding, Mingos & Powell (1993), Harding & Kariuki (1994), and Harding, Kariuki, Cernik & Cressey (1994).

2.3.2. Parallel-beam geometries, synchrotron radiation

The radiation from the X-ray tube is divergent and various methods can be used to obtain a parallel beam as shown in Fig. 2.3.2.1. Symmetrical reflection from a flat crystal is the usual method. An asymmetric reflecting monochromator with small incidence angle and large exit angle expands the beam, or in reverse condenses it (§2.3.5.4.1). A channel monochromator has the advantage of not changing the beam direction. A receiving slit or preferably Soller slits can be used to define the diffracted beam. A graphite monochromator in the diffracted beam or a solid-state detector eliminates fluorescence. The incident-beam

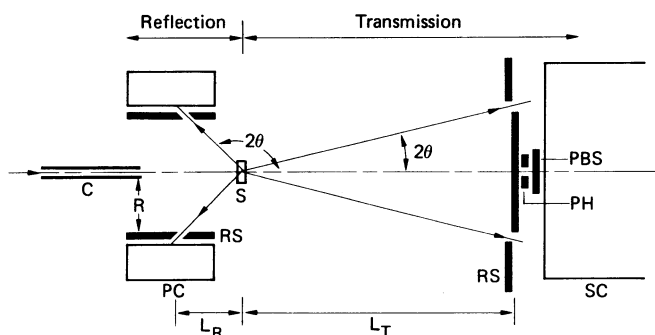


Fig. 2.3.1.15. Rigaku microdiffractometer for microanalysis. *C* collimator, *PC* ring proportional counter, *RS* ring slit with radius r , *S* specimen, *SC* scintillation counter, *PBS* primary beam stop, *PH* pinhole for alignment, L specimen-to-receiving-slit distance.

parallel slits limit vertical divergence. However, all the methods result in a large loss of intensity compared with conventional focusing. In contrast, the storage ring produces a virtually parallel beam with very small vertical divergence of about 0.1 mrad, and the monochromator is used only to select the wavelength. The rest of this section assumes a synchrotron-radiation source.

Storage-ring X-ray sources have a number of unique properties that are of great importance for powder diffraction. The advantages of synchrotron powder diffraction have been described by Hastings, Thomlinson & Cox (1984), Parrish & Hart (1987), Parrish (1988), and Finger (1989). Excellent patterns with high resolution and high peak-to-back ground ratio have been reported. These include the orders-of-magnitude higher intensity and nearly uniform spectral distribution compared with X-ray tubes, the wide continuous range of selectable wavelengths, and the single profile that avoids the problems caused by $K\alpha$ doublets and β filters. Owing to major differences in the diffractometer geometries, comparisons of intensities with X-ray tube focusing methods cannot be predicted simply from the number of source photons.

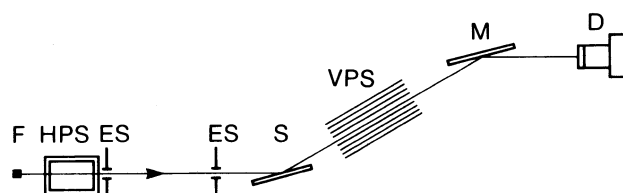


Fig. 2.3.2.1. Method to obtain parallel beam from X-ray tube for powder diffraction. HPS parallel slits to limit axial divergence, ES entrance slits (can be replaced by pair of flat parallel steel bars), *S* specimen, VPS parallel slits to define diffracted beam, *M* flat monochromator (can be omitted), *D* detector. See also Fig. 2.3.2.4(a).

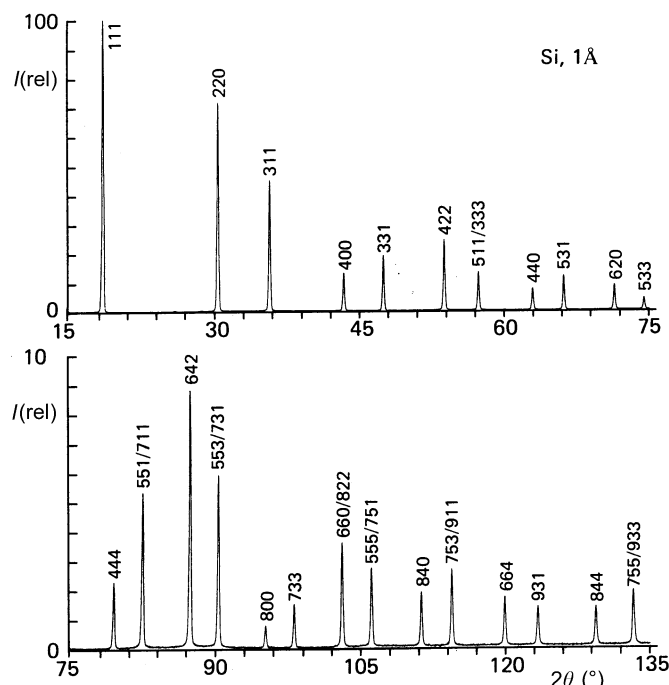


Fig. 2.3.2.2. Silicon powder pattern with 1 \AA synchrotron radiation using method shown in Fig. 2.3.2.4(a). The 444 reflection is the limit for $\text{Cu } K\alpha$ radiation.